Journal of Power Sources 195 (2010) 503–508

Contents lists available at ScienceDirect

Journal of Power Sources

journal homepage: www.elsevier.com/locate/jpowsour

Performance of micro-PEM fuel cells with different flow fields

Yuhao Lu, Ramana G. Reddy*

Department of Metallurgical and Materials Engineering, The University of Alabama, Tuscaloosa, AL 35487, USA

ARTICLE INFO

Article history:
Received 26 May 2009
Received in revised form 1 July 2009
Accepted 2 July 2009
Available online 10 July 2009

Keywords:
Micro-fuel cell
Flow field
Performance
PEMFC
Flooding

ABSTRACT

Four designs of flow fields were applied to micro-proton exchange membrane fuel cells (μ-PEMFCs) using microelectromechanical system (MEMS) technology. The flow fields and membrane electrolyte assembly (MEA) of 2.25 cm^2 active area were assembled to μ-PEMFCs. Electrochemical behaviors of these μ-PEMFCs were investigated by polarization method at reactants flow rates of 15 ml min^{-1}, 30 ml min^{-1} and 50 ml min^{-1}, respectively. This study emphasized the effects of different topologies of flow fields on performance of μ-PEMFCs. Results demonstrated that μ-PEMFCs with different flow fields have similar behavior at reactants flow rates of 50 ml min^{-1}. However, at reactants flow rates of 15 ml min^{-1} and 30 ml min^{-1}, performance of the μ-PEMFC with long and narrow micro-channels rapidly deteriorated due to the flooding in micro-channels. The mixed serpentine design had a good ability to resist the flooding, but it displayed a low maximum power density because of its short effective length of micro-channels. The results in this study suggested that the μ-PEMFC with a mixed multichannel design flow field and long micro-channels yielded the best performance.

1. Introduction

Micro-fuel cells (μ-FCs) have been recognized as promising electrochemical power sources in portable electronic devices due to their safety, high efficiency, renewable fuel and environmental compatibility. Although a lot of efforts have been made to improve the performance of μ-FCs, the development of μ-FCs still confront many technical challenges, including: (1) structural design, (2) fabrication, (3) gas diffusion layer (GDL) and catalyst layer (CL) optimization, (4) catalysts development and (5) membrane improvement.

The presence of μ-FCs benefited from the use of microelectromechanical system (MEMS) technology [1]. Basing on different materials, such as silicon [2–4], metals [5,6] and polymer [7,8], bipolar/end plates (BPs) with micron channels can be fabricated using MEMS for μ-FCs. Apart from MEMS technology, wire electro-discharge machining (WEDM) [9] and printed-circuit board (PCB) technology [10,11] were also introduced to fabricate μ-FCs. In order to simplify the fabrication process, Stanley et al. [12] developed a hybrid technique that combined the micro- and macro-machining technologies to create fuel cells in the 1–20 cm^3 range. Along with these technologies to be applied to the fabrication of μ-FCs, new structures for μ-FCs were designed as well. A monolithic structure was used in a single μ-FC [3], but a "flip-flop" structure was adopted in the stack of μ-FCs [13]. Qiao et al. [14] directly deposited catalysts on Flemion® tubes of the polymer electrolyte and obtained the μ-FCs. Chobanm Larry et al. [15] discussed a novel concept of the microfluidic fuel cell with the multi-stream laminate flow. Additionally, some new technologies were developed as well, such as the electrolyte membrane [16,17], electrode [18] and membrane electrode assembly (MEA) [19]. Our group has developed novel catalysts for micro-direct methanol fuel cells (μ-DMFCs) [20–22].

Performance of a fuel cell depends on all its components. However, Watkins et al. [23] reported that the output power density of fuel cell could be increased as much as 50% just by appropriate flow fields. These flow fields distribute the reactant gases evenly over the electrode surface to minimize the concentration overpotential [24]. Design of flow fields for fuel cells generally includes the geometrical configuration, channel and rib dimensions (depth and width) [25–30]. So far many flow fields have been designed and optimized to be successfully applied to conventional fuel cells. Nevertheless, they may not be appropriately applicable to μ-FCs [3,31]. Cha et al. [32] attributed the difference between conventional fuel cells and μ-FCs to scaling phenomena in conjunction with the oxygen distribution in the cathode flow channels and gas diffusion layer. Hsieh et al. [31,33–35] investigated the performance of μ-proton exchange membrane fuel cells (μ-PEMFCs) with different flow fields. Results showed that interdigitated flow field provided the best performance for μ-PEMFCs comparing serpentine, parallel and mesh flow fields. As for the serpentine flow field, the channel-to-rib ratio of 1.0 displayed the largest power output. However, considering the ratio of power gain to power consumption, the channel-to-rib ratio of 0.67 is a good choice.

* Corresponding author. Tel.: +1 205 348 4246; fax: +1 205 348 2164.
E-mail address: rreddy@eng.ua.edu (R.G. Reddy).

0378-7753/$ – see front matter © 2009 Elsevier B.V. All rights reserved.
doi:10.1016/j.jpowsour.2009.07.003

Our previous work [36] indicated the particular behaviors of μ-PEMFCs by the experimental and modeling methods. Assembling mode and flow field of the μ-PEMFC drastically affect its performance. Based on our previous results, we designed and fabricated four kinds of flow fields with different topologies for μ-PEMFCs. After assembled with these flow fields, performances of μ-PEMFCs were investigated and evaluated in this study. Unlike other papers [31,33–35], this study emphasized effects of flow fields on the performance of μ-PEMFCs based on topologies of flow fields other than the channel-to-rib ratios. In addition, effects of different topologies of flow fields on flooding of μ-PEMFCs were discussed as well.

2. Experimental

2.1. Fabrication of flow fields for μ-PEMFCs

MEMS technology was employed in this study to fabricate the flow fields on silicon wafers. The process has been described in our previous work [36,37]. Briefly, a coated 2.4 μm thick layer of Shipley 1818 photoresist, the first side of the silicon wafer was patterned by MA6/BA6 Mask aligner using the mask of inlet and outlet, and then etched in a STS Advanced Silicon Etcher (ASE). Once the etching was complete, the wafer was cleaned in preparation for the next step. The other side of the silicon wafer was coated with a 10 μm thick layer of Shiley Megaposit 220-7 photoresist. Then, double-sided alignment technology was used to accurately locate the patterns of flow fields on the photoresist layer according to the positions of inlets and outlets on the first side of the wafer. After the wafer was etched and cleaned, thin films of chromium and gold (20 nm and 0.2 μm) metals were deposited on the side as current collector using Denton vacuum E-beam evaporator. Fig. 1 displays these four kinds of flow fields on the silicon wafer.

Design 1 is the flow field of multichannel serpentine with mixing suggested by Cavalca et al. [38]. It was initially introduced into μ-FCs by Yen et al. [39]. Subsequently, Lu et al. [40] investigated its behavior in μ-DMFCs in detail. However, so far this design has not been reported to be used in μ-PEMFCs. Designs 2 and 3 are conventional single- and two-channel serpentine designs, respectively. Design 4 is one type of mixed serpentine flow fields. Although design 4 was successfully developed by our group for conventional PEMFCs [41], it is the first time that design 4 is applied to the μ-PEMFC. Table 1 lists the geometric parameters of these four flow fields. An example is shown in Fig. 2 to explain the dimensions of flow fields [36].

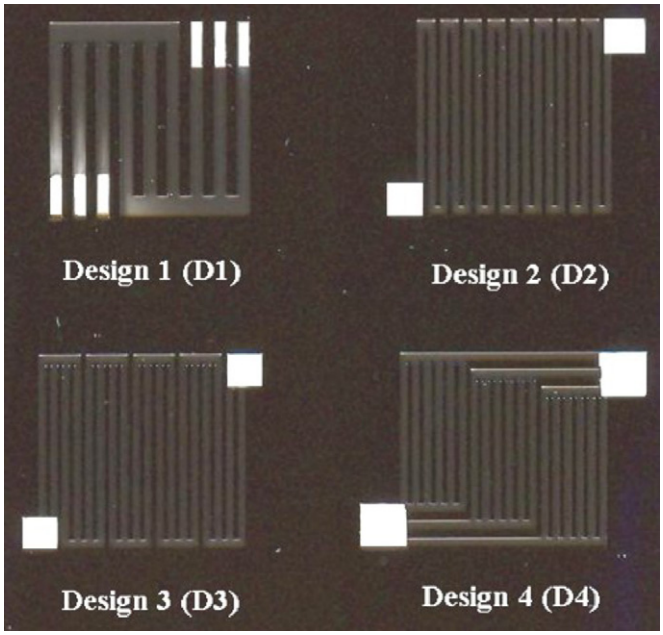

Fig. 1. Four designs of flow fields for μ-PEMFCs.

Table 1
Geometric parameters of the flow fields.

	Design 1	Design 2	Design 3	Design 4
Channel width (μm)	750	375	375	375
Rib width (μm)	750	375	375	375
Channel depth (μm)			300	
Channel length (mm)			12.75	
Current collector of Cr/Au (nm/μm)			20/0.2	

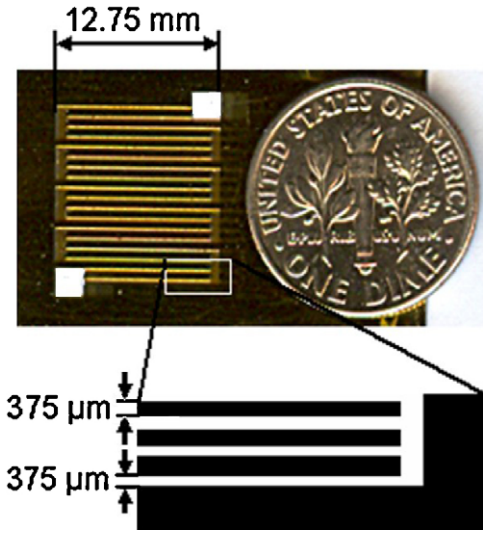

Fig. 2. Dimensions of design 3 with current collector.

2.2. Assembly of μ-PEMFCs

Two BPs with the same flow field and an electrode membrane assembly (MEA) were assembled to a μ-PEMFC. The sandwich structure of MEA consisted of Nafion® membrane and two electrodes. Nafion® 112 was used in the MEA, previously treated by aqueous solution 3% hydrogen peroxide and 1 M sulfuric acid. In order to weaken the effect of electrodes on the performance of μ-PEMFC, a high catalyst loading with optimized Nafion® content was used in the μ-PEMFCs. In case of CO poisoning, the alloy of Pt/Ru was employed as anodic catalyst in the μ-PEMFCs. The active areas of all electrodes in the μ-PEMFCs are 1.5 cm × 1.5 cm. The anode (ETEK, 5 mg cm^{-2} Pt/Ru 1:1), the cleaned Nafion® 112 membrane, and the cathode (ETEK, 5 mg cm^{-2} Pt) were pressed with a pressure of 40 kg cm^{-2} at 150 °C for 2.5 min to get a sandwiched MEA.

2.3. Measurement of μ-PEMFCs

μ-PEMFCs are being developed as a promising electrochemical power to replace the lithium batteries in portable electronic devices, such as cell phone, laptop computer, and GPS. Generally, these portable devices are operated at room temperature. Thus, in the study μ-PEMFCs were evaluated at room temperature (20 ± 1 °C) with 100% humidified reactant gases. Gas flow meters were used to feed hydrogen and air to μ-PEMFCs. Three flow rates of hydrogen/air, 15/15 ml min^{-1}, 30/30 ml min^{-1}, and 50/50 ml min^{-1}, were used to investigate performance of μ-PEMFCs. The polarization experiments of the μ-PEMFCs were conducted by the AMREL Zero-volt eLoad (ZVL60-10-20L). After stabilizing at a current for 2 min, the corresponding potential of the μ-PEMFC was

Table 2
Properties of air flowing through μ-PEMFCs.

	Design 1	Design 2	Design 3	Design 4
Effective channel length/mm	38.25	212.25	116.25	22.88
Hydraulic diameter (D_H)/mm	0.43	0.33	0.33	0.43/0.33[a]
Reynolds number (Re)	10.65	49.72	24.86	10.65/27.62[a]
Knudsen number	1.5×10^{-4}	1.9×10^{-4}	1.9×10^{-4}	$1.5 \times 10^{-4}/1.9 \times 10^{-4}$[a]
Friction factor	6.16	1.16	2.32	6.16/2.09[a]
Pressure drop/Pa	106	5484	1423	42

[a] Ends of channels/middle of channels.

recorded. Eventually, the polarization curves were obtained from the recorded data.

After feeding with the humidified reactant gases (RH = 100%) for 1 h, resistance of μ-PEMFCs was measured by CHI 660A with the AC impedance technology. A sinusoidal signal with amplitude of 5 mV was applied to the μ-PEMFCs. The frequency of the signal was scanned from 100 kHz to 0.1 Hz at an applied potential of 0.0 V. The real part of impedance was recorded as resistance of the μ-PEMFC when its imaginary part is zero.

Flooding in μ-PEMFCs was studied using the method of "over-saturated vapor" in order to aggravate the process of flooding. The "over-saturated" means that the relative humidity (RH) of gases is greater than 100% when gases just enter the μ-PEMFC. The μ-PEMFCs were kept in the atmosphere of $20 \pm 1\,^{\circ}C$, but the temperature of the humidity system was increased to 35 °C. The current of 400 mA was applied to the μ-PEMFCs, and the potential of the μ-PEMFCs was recorded along with the time.

3. Results and discussion

Flow fields determine the distributions of reactant gases in μ-PEMFCs, and further affect performance of μ-PEMFCs. In the PEM fuel cells, fuel and air arrive at catalyst layers through flow fields, and the electricity power is generated. During the process, the cathode sides become a key factor that has impact on performance of PEM fuel cells because of the slow kinetics of oxygen reduction reaction (ORR) and the mass transport limitation caused by liquid water. In the cathode, the slow kinetics of ORR results in more than 90% of overpotential in the μ-PEMFC [36]. Moreover, the ORR and electro-osmotic drag bring liquid water into cathode. Liquid water accumulates in the micro-channels and the porous GDLs and CLs, namely water flooding. The water flooding hinders oxygen moving in the micro-channels and accessing to the active sites, which deteriorates performance of μ-PEMFCs. Table 2 summarizes the properties of humidified air of 15 ml min^{-1} flowing

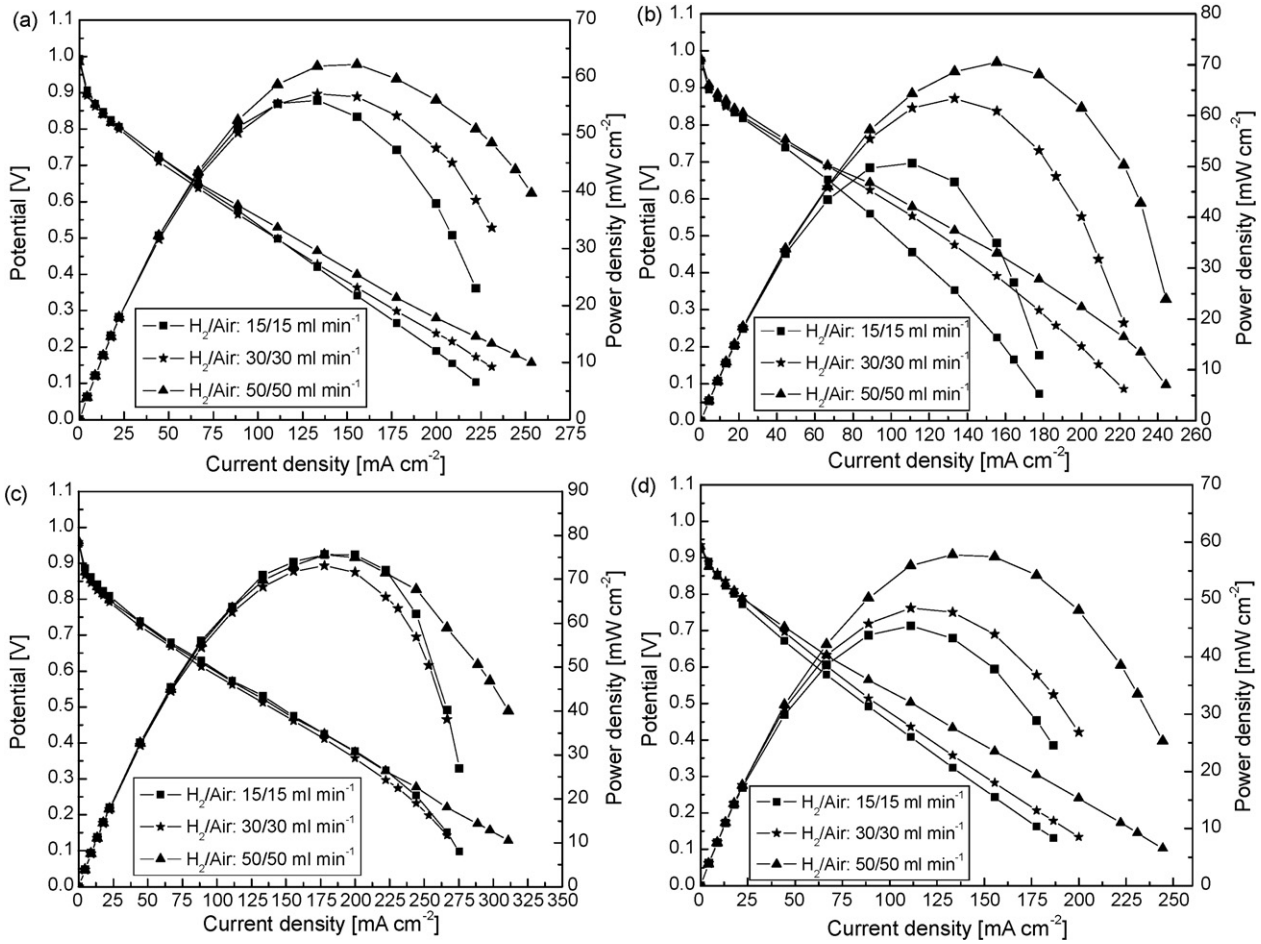

Fig. 3. Polarization curves of μ-PEMFCs with different flow fields. (a) Design 1; (b) design 2; (c) design 3; and (d) design 4.

Table 3
Maximum power densities of μ-PEMFCs at different gases flow rates.

Flow rate (ml min^{-1})	Maximum power density (mW cm^{-2})			
	Design 1	Design 2	Design 3	Design 4
15	55.81	50.79	75.97	45.26
30	56.95	63.58	73.44	48.72
50	62.38	70.55	75.97	57.77

through the cathodic sides of μ-PEMFCs. These numbers were calculated according to the equations described in Ref. [42]. It is worth noticing that the conventional equation used in this study to calculate the friction factor is applicable to micro-channels [43]. In the table, effective channel length was defined as the shortest distance through which the gases (hydrogen and air) passed from an inlet to an outlet in a flow field.

Fig. 3 shows a series of cell polarization curves operated at different flow rates of reactant gases. The hydrogen flow rates were 15 ml min^{-1}, 30 ml min^{-1} and 50 ml min^{-1} corresponding to stoichiometric numbers of 3, 6 and 10 at the reference current of 0.3 A cm^{-2}. The same air flow rates were used, but its stoichiometric numbers were 1.27, 2.54 and 4.23, respectively. A higher flow rate keeps a higher concentration of the reactant in the catalyst layer, furthermore, causes a larger pressure gradient to enhance mass transfer by forced convection. As shown in Fig. 3(a), the polarization curves of design 1 with wide channels display two parts, kinetic and ohmic polarization, while the mass transport limitation is not apparently observed. The performance of design 1 was improved with the increase of flow rates of gases. Its maximum power densities at different gases flow rates were summarized in Table 3. Designs 2 and 3 are single- and double-channel serpentine design, respectively. Their long effective channels made an adverse effect on the mass transport which was clearly exhibited in the polarization curves of designs 2 and 3. As to design 2, the increase of flow rate drastically improved its performance. Especially, its power density increased 25.2% when the reactant gases flow rates raised from 15 ml min^{-1} to 30 ml min^{-1}. However, the change in gases flow rates did not significantly influence the performance of design 3. The high flow rate only enhanced the power density of design 3 at high current densities. Adding the number of channel, design 4 reduced the effect of narrow channels on the mass transport limitation. The part of concentration polarization became indistinct in the polarization curves of design 4 as shown in Fig. 3(d).

The polarization curves of μ-PEMFCs were affected by their resistance as well. When μ-PEMFCs were fully humidified, difference in their resistance might come from the contacting parts of flow fields and electrodes. The contact resistance depends on the assembling pressure and contact area. Due to the fragile nature of silicon wafer and thin current collectors, μ-PEMFCs in the study have the large resistance to which the contact between current collectors and electrodes contributes 20% [36]. The large resistance would change the distributions of current and overpotential. Fig. 4 describes the resistance of μ-PEMFCs obtained from electrochemical impedance spectroscopy. In order to compare the effect of different flow fields on the mass transport, the polarization curves of μ-PEMFCs were corrected by removing ohmic losses. The corrected polarization curves are shown in Fig. 5.

After removing ohmic resistance, the corrected polarization curves only reflect two control processes, namely kinetic and mass transport controls. The kinetic control attributes to the properties of MEA, but the mass transport control was determined by flow fields and porous media to a large extent. As shown in Fig. 5, different flow fields bring different performances to μ-PEMFCs. However, difference in performance of μ-PEMFCs gradually decreased with increasing gases flow rates. When μ-PEMFCs worked at 150 mA cm^{-2} and the flow rates of reactant gases were

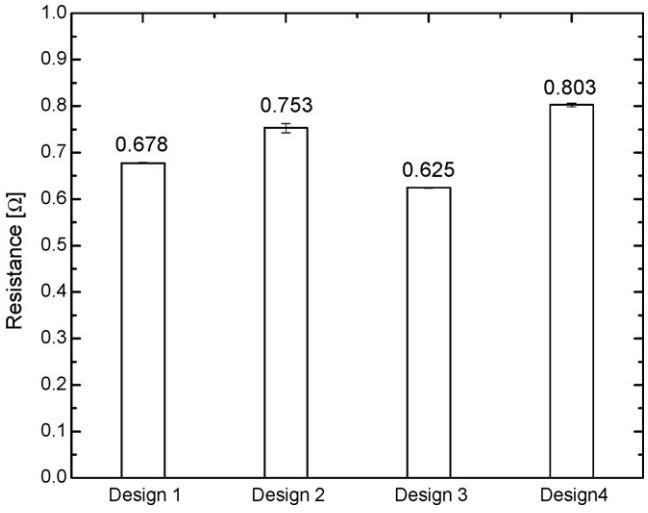

Fig. 4. Resistance of μ-PEMFCs with different flow fields.

15 ml min^{-1}, they generated the power densities covering from 76 mW cm^{-2} to 105 mW cm^{-2} which resulted about 38% discrepancy. Difference is 21% at gases flow rates of 30 ml min^{-1}, and 13% at gases flow rates of 50 ml min^{-1}. As mentioned above, a high flow rate will improve the mass transport in micro-channels by forced convection. Forced convection does not only compel gases to catalyst layers, but also makes gases span the ribs of micro-channels and disperses gases in the whole gas diffusion layers (GDL). The high dispersion of gases in GDL will remove the differences among μ-PEMFCs caused by different flow fields. When the gases flow rates were 50 ml min^{-1}, the produced liquid water was readily removed in the micro-channels and had a weak influence on the mass transport. Fig. 5(c) indicates that the flow fields with narrower micro-channels yield better performance, which is consistent with the results of Cha et al. [44]. A narrower channel helps the mass transport by reducing the dead zone and increasing gas flow velocity. When gases flow rates decreased, performance of design 2 rapidly deteriorated. The probable reason was the flooding blocking the mass transport in micro-channels. At low current density, μ-PEMFCs only produced a little liquid water that was not enough to result in the flooding, so the design 2 appeared to yield the best performance. However, with the liquid water accumulating in micro-channels, performance of design 2 became worse. Comparing with other flow fields, design 4 has a shortest effective length of micro-channel that only introduces a small pressure gradient in the flow field. Thus, the fluids in design 4 only include a weak convective character in the mass transport which leads to unfavorable performance. Decrease in gases flow rates gave prominence of mass transport limitation to polarization curves of μ-PEMFCs as shown in Fig. 5(a) and (b).

The mass transport limitation forced by liquid water is another important issue in μ-PEMFCs. Although a high gases flow rate will impede flooding from micro-channels and improve the mass transport, the process adds the parasitic energy for the μ-PEMFC systems. A good design of flow field for the μ-PEMFC should avoid the accumulation of liquid water in micro-channels and minimized barriers for mass transport at low gases flow rates. In the study, an extreme condition (RH = 250%) was employed to investigate the flooding in the μ-PEMFCs with different flow fields. When the gases humidified at 35 °C (RH = 250%) were fed to μ-PEMFCs with an atmosphere of 20 °C, the over-saturated water would condensate in the micro-channel of flow fields and degraded the mass transport. Fig. 6 describes the behavior of flooding in μ-PEMFCs with different flow fields. The flow rates of hydrogen and air were

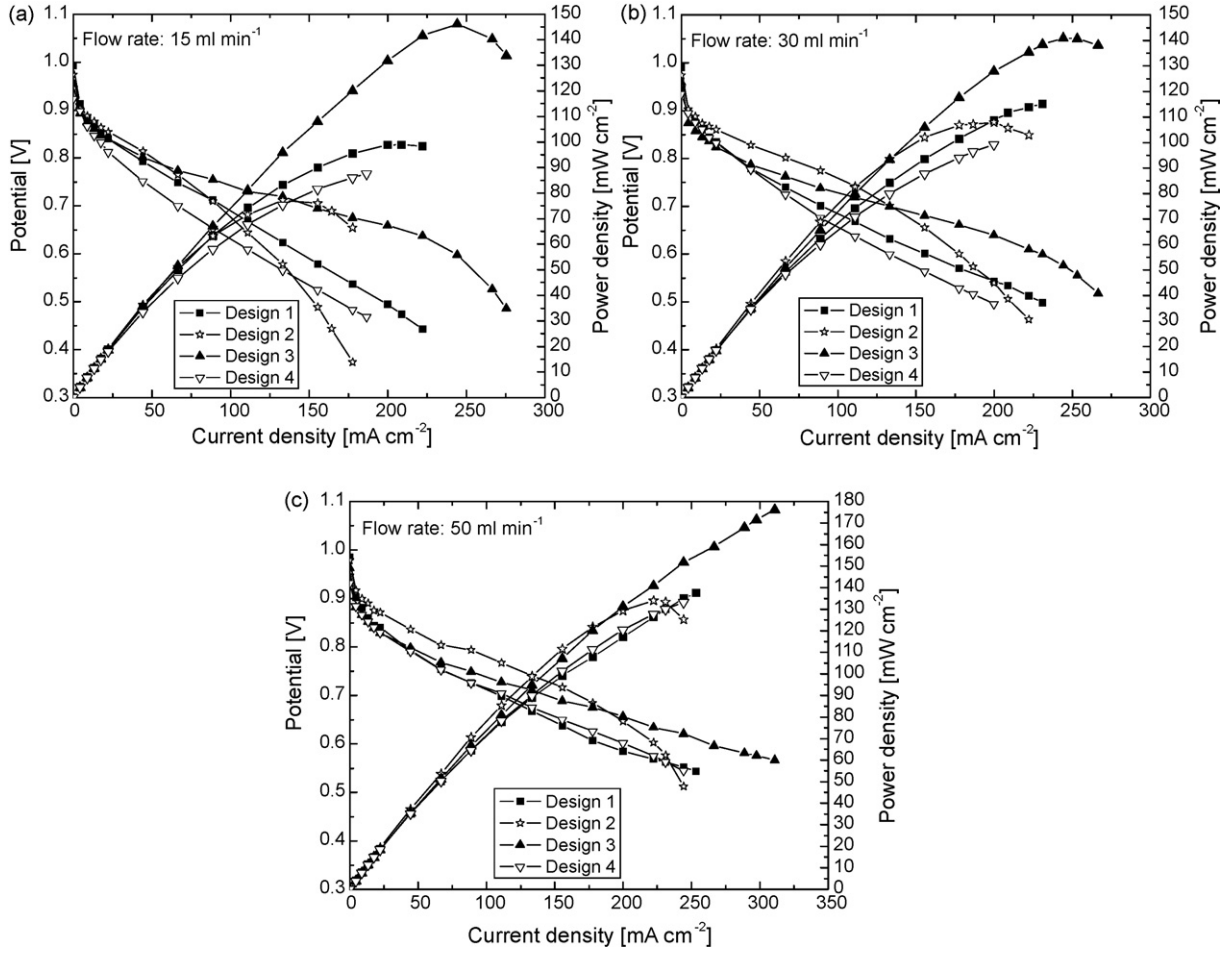

Fig. 5. IR-corrected polarization curves of μ-PEMFCs with different flow rates.

15 ml min^{-1} and the currents of μ-PEMFCs were kept at 400 mA. In order to easily compare the flooding in μ-PEMFCs with different flow fields, the relative values of potentials were adopted. Assuming that the potential was 100% at the beginning, and the other potentials were expressed by percentage relative to the initial potential. The potential of design 2 decreased to 40% from 100% in 4 min. Long channel length with the narrow open area is susceptible to flooding. Even though the two-channel serpentine design was used in the μ-PEMFC, the time when its potential decreased to 40% from 100% is 7 min, only 3 min more than that in design 2. Short channel length and wide open area improve the flooding of the μ-PEMFC in design 1. After operating for more than 25 min, its potential was about 64%. The potential of design 4, a mixed serpentine design with multichannel, decreased to 52% at the first 8 min. The decrease in potential implied that the liquid water was forming and accumulating in narrower part of the flow field. Performance of the μ-PEMFC rapidly deteriorated. However, the liquid water was easily released from channels due to short effective channel length and multiple channels. It is observed that performance of the μ-PEMFC was recovered at the tenth minute. After that time, the potential of the μ-PEMFC kept at 90%, and repeated the recovery process at about 20 min. As a whole, design 4 appeared to have the best ability to resist the flooding.

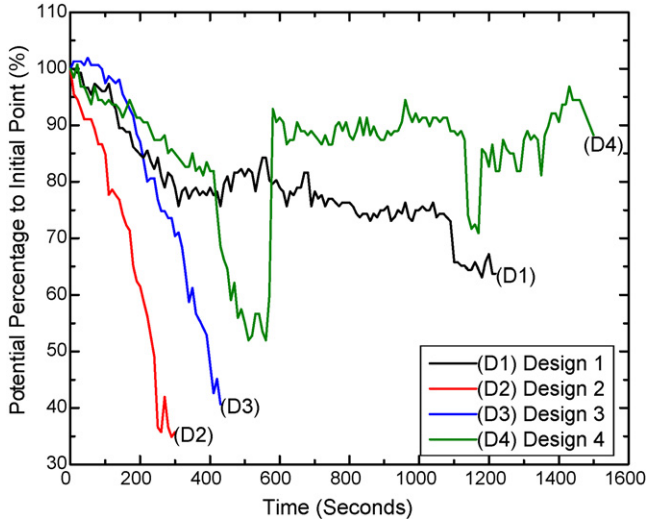

Fig. 6. Change in potential with time at cell currents of 400 mA.

4. Conclusions

Flow fields play a very important role in the performance of μ-PEMFCs. A good design of the flow field can not only provide uniform distributions of gases in electrodes to improve the performance of μ-PEMFCs but also enhance the ability to recover from the flooding. This study investigated performances of μ-PEMFCs with four kinds of flow fields manufactured by MEMS technology. These flow fields have different topologies, channel and rib width, and effective channel length. The flow field with narrow and long channel presented a good performance at high gases flow rates. High flow rates forced the convective mass transport and impeded the

flooding in micro-channels and porous materials, which improved performance of μ-PEMFCs. However, with the flow rates decreasing, the long and narrow channels were susceptible to flooding by the produced liquid water and its performance rapidly deteriorated. The mixed serpentine design had a good ability to resist the flooding. But its short effective length of channels only led to a small pressure gradient and a small convective character in mass transport, which caused a bad performance in its polarization curves. The results suggest that the μ-PEMFC with good performance should use the flow field with a mixed multichannel design and long microchannels.

Comparing with the polarization curves before and after correction of ohmic resistance, the resistance wasted almost half the power density generated by μ-PEMFCs at $20 \pm 1\ ^{\circ}C$. Therefore, optimization of the assembling structure of μ-PEMFCs to decrease the resistance will be an important issue for our future work.

Acknowledgements

Authors are pleased to acknowledge the financial support provided by Alabama EPSCoR graduate research scholars program, ACIPCO, and the University of Alabama. We are grateful to Dr. Alton Highsmith of Central Analytical Facility-Clean Room Group for his assistance in MEMS fabrication and the assistance of Mr. Wei Li in the discussion of fuel cells testing. We also thank Dr. Divakar Mantha for reviewing the paper.

References

[1] Y. Yamazaki, J. Power Sources 50 (2004) 663–666.
[2] S. Motokawa, M. Mohamedi, T. Momma, S. Shoji, T. Osaka, Electrochem. Commun. 6 (2004) 562–565.
[3] J.P. Meyers, H.L. Maynard, J. Power Sources 109 (2002) 76–88.
[4] J. Yu, P. Cheng, Z. Ma, B. Yi, Electrochim. Acta 48 (2003) 1537–1541.
[5] R. Hahn, S. Wagner, A. Schmitz, H. Reichl, J. Power Sources 131 (2004) 73–78.
[6] S. Hsieh, C. Feng, C. Huang, J. Power Sources 163 (2006) 440–449.
[7] H. Cha, H. Choi, J. Nam, Y. Lee, S. Cho, E. Lee, J. Lee, C. Chung, Electrochim. Acta 50 (2004) 795–799.
[8] K. Shah, W.C. Shinl, R.S. Besser, Sens. Actuators B 97 (2004) 157–167.
[9] M.A. Müller, C. Müller, R. Förster, W. Menz, Microsyst. Technol. 11 (2005) 280–281.
[10] A. Schmitz, M. Tranitz, S. Wagner, R. Hahn, C. Hebling, J. Power Sources 118 (2003) 162–171.
[11] Ryan O'Hayere, Daniel Braithwaite, Weston Hermann, Sang-Joon Lee, Tibor Fabian, Suk-Won Cha, Yuji Saito, B. Fritz, Prinz, J. Power Sources 124 (2003) 459–472.
[12] K.G. Stanley, E.K. Czyzewska, T.P.K. Vanderhoek, L.L.Y. Fan, K.A. Abel, Q M Jonathan, M Wu, (Ash) Parameswaran, J. Micromech. Microeng. 15 (2005) 1979–1987.
[13] S.J. lee, A. Chang-Chien, S.W. Cha, R. O'Hayre, Y.I. Park, Y. Saito, F.B. Prinz, J. Power Sources 112 (2002) 410–418.
[14] H. Qiao, H. Shiroishi, T. Okada, J. Power Sources 139 (2005) 30–34.
[15] E.R. Chobanm Larry, J. Markoski, Andrzej Wieckowski, J.A. Paul, Kenis, J. Power Sources 128 (2004) 54–60.
[16] L. Mex, J. Müller, Membr. Technol. 115 (1999) 5–9.
[17] T. Pichonat, B. Gauthier-Manuel, D. Hauden, Fuel Cells Bull. 2004 (8) (2004) 11–14.
[18] A.D. Taylor, B.D. Lucas, L.J. Guo, L.T. Thompson, J. Power Sources 171 (2007) 218–223.
[19] C. Feng, P.C.H. Chan, I. Hsing, Fuel Cells Bull. 2007 (2) (2007) 12–15.
[20] Y. Lu, R.G. Reddy, Electrochim. Acta 52 (2007) 2562–2569.
[21] Y. Lu, R.G. Reddy, Int. J. Hydrogen Energy 33 (2008) 3930–3937.
[22] Y. Lu, R.G. Reddy, ECS Trans. 6 (2008) 105–116.
[23] D.S. Watkins, K.W. Dircks, US Patent No. 5,108,849 (1992).
[24] X. Li, I. Sabir, Int. J. Hydrogen Energy 30 (2005) 359–371.
[25] E. Hontañón, M.J. Escudero, C. Bautista, P.L. Garcia-Ybarra, L. Daza, J. Power Sources 86 (2000) 363–368.
[26] A. Kumar, R.G. Reddy, J. Power Sources 113 (2003) 11–18.
[27] W. Yan, C. Yang, C. Soong, F. Chen, S. Mei, J. Power Sources 160 (2006) 284–292.
[28] K. Hongthong, K. Pruksathorn, P. Piumsomboon, P. Sripakagorn, Korean J. Chem. Eng. 24 (2007) 612–617.
[29] D.H. Jeon, S. Greenway, S. Shimpalee, J.W. Van Zee, Int. J. Hydrogen Energy 33 (2008) 1052–1066.
[30] X.Q. Xing, K.W. Lum, H.J. Poh, Y.L. Wu, J. Power Sources 186 (2009) 10–21.
[31] S. Hsieh, S. Yang, J. Kuo, C. Huang, H. Tsai, Energy Convers. Manage. 47 (2006) 1868–1878.
[32] S.W. Cha, R. O'Hayre, Y. Saito, F.B. Prinz, J. Power Sources 134 (2004) 57–71.
[33] S. Hsieh, S. Yang, C. Feng, J. Power Source 162 (2006) 262–270.
[34] S. Hsieh, K. Chu, J. Power Sources 173 (2007) 222–232.
[35] S. Hsieh, Y. Huang, J. Power Sources 183 (2008) 193–204.
[36] Y. Lu, R.G. Reddy, Electrochim. Acta 54 (2009) 3952–3959.
[37] Y. Lu, R.G. Reddy, Supplemental Proceedings: Volume 2: Materials Characterization, Computation and Modeling, TMS (The Minerals, Metals & materials Society), 2009, pp. 161–167.
[38] C. Cavalca, S.T. Homeyer, E. Walsworth, U.S. Patent No. 5,686,199 (1997).
[39] T.J. Yen, N. fang, X. Zhang, G.Q. Lu, C.Y. Wang, Appl. Phys. Lett. 83 (2003) 4056–4058.
[40] G.Q. Lu, C.Y. Wang, T.J. Yen, X. Zhang, Electrochim. Acta 49 (2004) 821–828.
[41] A. Kumar, R.G. Reddy, In: D. Chandra, R.G. Bautista (Eds.), TMS, Warrendale, 2002, pp. 41–53.
[42] F. Barbir, PEM Fuel Cells: Theory and Practice, Elsevier Academic Press, Burlington, MA, 2005, pp. 170–177.
[43] P. Wu, W.A. Little, Cryogenics 23 (1983) 273–277.
[44] S.W. Cha, R. O'Hayre, Y. Park, F.B. Prinz, J. Power Sources 161 (2006) 138–142.